Heave-Plate Hydrodynamic Coefficients for Floating Offshore Wind Turbines – A Compilation of Data

Preprint

Matthew Turner,[1] Lu Wang,[1] Krish Thiagarajan,[2] and Amy Robertson[1]

1 National Renewable Energy Laboratory
2 University of Massachusetts Amherst

Presented at the ASME 2023 5th International Offshore Wind Technical Conference
Exeter, United Kingdom
December 18–19, 2023

NREL is a national laboratory of the U.S. Department of Energy
Office of Energy Efficiency & Renewable Energy
Operated by the Alliance for Sustainable Energy, LLC

This report is available at no cost from the National Renewable Energy Laboratory (NREL) at www.nrel.gov/publications.

Contract No. DE-AC36-08GO28308

Conference Paper
NREL/CP-5000-87275
January 2024

Heave-Plate Hydrodynamic Coefficients for Floating Offshore Wind Turbines – A Compilation of Data

Preprint

Matthew Turner,[1] Lu Wang,[1] Krish Thiagarajan,[2] and Amy Robertson[1]

1 National Renewable Energy Laboratory
2 University of Massachusetts Amherst

Suggested Citation
Turner, Matthew, Lu Wang, Krish Thiagarajan, Amy Robertson. 2024. *Heave-Plate Hydrodynamic Coefficients for Floating Offshore Wind Turbines – A Compilation of Data: Preprint*. Golden, CO: National Renewable Energy Laboratory. NREL/CP-5000-87275. https://www.nrel.gov/docs/fy24osti/87275.pdf.

NREL is a national laboratory of the U.S. Department of Energy
Office of Energy Efficiency & Renewable Energy
Operated by the Alliance for Sustainable Energy, LLC

This report is available at no cost from the National Renewable Energy Laboratory (NREL) at www.nrel.gov/publications.

Contract No. DE-AC36-08GO28308

Conference Paper
NREL/CP-5000-87275
January 2024

National Renewable Energy Laboratory
15013 Denver West Parkway
Golden, CO 80401
303-275-3000 • www.nrel.gov

NOTICE

This work was authored in part by the National Renewable Energy Laboratory, operated by Alliance for Sustainable Energy, LLC, for the U.S. Department of Energy (DOE) under Contract No. DE-AC36-08GO28308. Funding provided by the U.S. Department of Energy Office of Energy Efficiency and Renewable Energy Wind Energy Technologies Office. The views expressed herein do not necessarily represent the views of the DOE or the U.S. Government. The U.S. Government retains and the publisher, by accepting the article for publication, acknowledges that the U.S. Government retains a nonexclusive, paid-up, irrevocable, worldwide license to publish or reproduce the published form of this work, or allow others to do so, for U.S. Government purposes.

Cover Photos by Dennis Schroeder: (clockwise, left to right) NREL 51934, NREL 45897, NREL 42160, NREL 45891, NREL 48097, NREL 46526.

NREL prints on paper that contains recycled content.

HEAVE-PLATE HYDRODYNAMIC COEFFICIENTS FOR FLOATING OFFSHORE WIND TURBINES – A COMPILATION OF DATA

Matthew Turner
National Renewable Energy Laboratory
Golden, CO

Lu Wang
National Renewable Energy Laboratory
Golden, CO

Krish Thiagarajan
University of Massachusetts
Amherst, MA

Amy Robertson
National Renewable Energy Laboratory
Golden, CO

ABSTRACT

The National Renewable Energy Laboratory's OpenFAST software is utilized by academics and industry professionals alike to simulate offshore wind turbines. The software's modeling of hydrodynamic loads on heave plates attached to these structures relies on user-specified hydrodynamic coefficients. To guide the proper selection of these coefficients and potentially develop a new functionality within OpenFAST that automatically prescribes and/or adjusts the heave-plate hydrodynamic coefficients, we review past literature to examine the dependence of the added mass, damping, and drag coefficients on various relevant nondimensional parameters, including the Keulegan-Carpenter number, the frequency parameter, and the plate thickness ratio. Existing data in the literature show strong dependence of the hydrodynamic coefficients on the Keulegan-Carpenter number. We observe consistent trends across a range of different plate geometry, plate porosity, and flow conditions. Secondary dependence of the coefficients on the frequency parameter and plate thickness ratio is also present.

Keywords: hydrodynamics, heave plate, added mass, drag, damping

NOMENCLATURE

a	Amplitude of oscillation
A_{33}	Added mass in heave
B_{33}	Damping coefficient in heave
B_{eq}	Equivalent linear damping coefficient
C_{33}	Hydrostatic stiffness in heave
C_A	Nondimensional added-mass coefficient
C_B	Nondimensional damping coefficient
C_D	Drag coefficient
D_h	Plate hydraulic diameter
D_c	Diameter of attached cylinder
f	Frequency of oscillation
F_3	External force in heave
F_z	Hydrodynamic force in heave
KC	Keulegan-Carpenter number
M	Structure mass
M'	Reference mass
Re	Reynolds number
S	Plate area
t'	Plate thickness ratio
t_p	Plate thickness
β	Frequency parameter
ν	Kinematic viscosity of fluid
ρ	Density of fluid
ω	Angular frequency of oscillation

1. INTRODUCTION

Multicolumn substructures are a common type of floating support for offshore wind turbines. Designs like the WindFloat currently deployed off the coast of Portugal use a flat plate structure at the column base—called a heave plate—to attenuate platform motion (see Figure 1). In the oil and gas industry, heave plates are normally not used in conjunction with semi-submersibles. They are, however, common with monocolumn spar platforms that support vertical risers, which need to minimize heave motion.

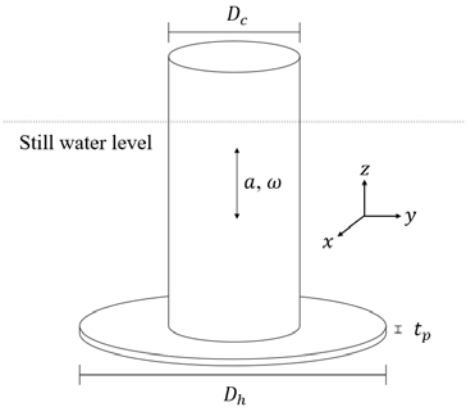

FIGURE 1: ILLUSTRATION OF A CYLINDER WITH A HEAVE PLATE ATTACHED OSCILLATING IN THE HEAVE DIRECTION.

TABLE 1: A SUMMARY OF THE REFERENCES SELECTED FOR THE PRESENT REVIEW

Reference	Method	Number of plates	Plate geometry	Plate porosity	Attached to cylinder[1]	Motion	Data	Effects considered
An & Faltinsen [1]	Numerical/ experimental	1	Rectangular	Yes	No	Forced oscillation	C_A and C_B	KC, β, porosity ratio, plate depth
Bezunartea-Barrio et al. [2]	Experimental	1	Circular	No	Yes	Forced oscillation and free decay	C_A, C_B and C_D	KC, β, and different model scale
Li et al. [3]	Experimental	1-3	Square	Yes	No	Forced oscillation	C_A and C_D	KC, β, plate depth, plate thickness ratio, edge shape, porosity ratio
Liang et al. [4]	Experimental	1	Square	No	No	Forced oscillation	C_A and C_D	KC, β, plate thickness ratio
Liu et al. [5]	Experimental	1	Square	No	No	Forced oscillation	C_A and C_D	KC, β
Tao & Dray [6]	Experimental	1	Circular	Yes	No	Forced oscillation	C_A and C_D	KC, β, porosity ratio
Tao & Thiagarajan [7]	Numerical	1	Circular	No	Yes	Forced oscillation	C_B, and C_D	KC, thickness ratio
Tian et al. [8]	Experimental	1	Circular, octagon, hexagon, square	Yes	No	Forced oscillation	C_A and C_B	KC, β, plate shape, plate thickness ratio, edge corner radius, porosity ratio
Tian et al. [9]	Experimental	1-3	Circular, octagon, hexagon, square, rectangle, triangle	Yes	No	Forced oscillation	C_A and C_B	KC, β, plate shape, plate thickness ratio, edge corner radius, porosity ratio, multiple plates
Vu et al. [10]	Experimental	1	Circular	Yes	No	Forced oscillation	C_B	KC, β, porosity ratio
Wadhwa & Thiagarajan [11]	Experimental	1	Circular	No	No	Forced oscillation	C_A, C_B, and C_S (slamming coefficient)	KC, β, plate depth, slamming (time varying added mass with submergence)
Wadhwa et al. [12]	Experimental	1	Circular	No	No	Forced oscillation	C_A and C_B	KC, β, plate depth, seabed effects
Yang et al. [13]	Numerical	1	Circular	No	No	Forced oscillation	C_A and C_B	KC, plate thickness ratio, current

[1] Slender support is not considered.

Engineering models of heave plates typically rely on the tuning of hydrodynamic coefficients to correctly estimate the hydrodynamic loading to be applied across the entire plate. A large volume of experimental, numerical, and field data exists on three such coefficients—the added mass coefficient, C_A; damping coefficient, C_B; and drag coefficient, C_D—and their dependence on dimensionless numbers that characterize the design of the heave plate and the condition the heave plate is operating in. These numbers include the Reynolds number, Re; Keulegan-Carpenter number, KC (ratio of motion amplitude to plate characteristic dimension); the frequency parameter, β (the ratio of Re to KC); plate porosity ratio; and plate thickness ratio, t'. It is noted that through the process of linearization, the damping and drag coefficients can be related through the KC number.

Select literature from the past 30 years (see Table 1) was reviewed to compile data in order to determine general correlations between the hydrodynamic coefficients—C_A, C_B, and C_D—and the dimensionless parameters—KC, β, and t'. As shown in Table 1, most of the data shown in this review were derived from forced-oscillation experiments in heave, supplemented by some numerical data. Data for different plate

shapes, plate thickness ratios, plate porosity ratios, and levels of submergence are all included. Most of the references selected investigated the behavior of plates with small attachments for support, although circular plates with attached cylinders are considered as well (Figure 1). Circular plates with attached cylinders are of particular interest due to their geometric similarity to the columns of offshore wind turbine platforms.

To extract trends that are generally applicable to different heave-plate designs, we present and compare all data collected as functions of KC and β without controlling for other factors, apart from plate shape and t'.

Section 2 describes the modeling of heave-plate hydrodynamic loads. This includes the equations of motion used for structures in heave, the mathematical definition of the relevant coefficients, and the definitions and context behind KC and β. Section 3 presents the data from the literature and discusses the trends observed within that data. Section 4 summarizes the main findings and provides recommendations for future investigations.

2. METHODS

To enable more convenient modeling of floating offshore wind turbine platforms with heave plates, existing research and data on heave-plate loads have been compiled. This is to evaluate the possibility of developing, within OpenFAST, a functionality to automatically prescribe and adjust the hydrodynamic coefficients for different types of heave plates and for different conditions—especially the drag coefficient or an equivalent damping coefficient that cannot be estimated from potential-flow theory.

Consider the structure illustrated in Figure 1 that is oscillating in the vertical (heave) direction. With the assumption that the structure is neutrally buoyant at equilibrium ($\boldsymbol{z} = \boldsymbol{0}$), the equation of motion of the structure in heave can be written as

$$F_3 = (M + A_{33})\ddot{z} + B_{33}\dot{z} + \frac{1}{2}\rho C_D S\dot{z}|\dot{z}| + C_{33}z, \quad (1)$$

where $\boldsymbol{F_3}$ is the external force in the vertical direction applied to the structure. In forced-oscillation experiments in calm water, this is the force directly measured by the load cell. Equation (1) has separate terms for linear damping from, for example, wave radiation and wall friction, and quadratic form drag on the heave plate. Alternatively, the linear damping and quadratic form drag can be combined and approximated by an equivalent linear damping term as shown in Eq. (2):

$$F_3 = (M + A_{33})\ddot{z} + B_{eq}\dot{z} + C_{33}z. \quad (2)$$

For given amplitude, a, and angular frequency of oscillation, ω, B_{eq} is given by

$$B_{eq} = B_{33} + \frac{4}{3\pi}\rho a\omega C_D S. \quad (3)$$

Equation (3) can be derived from matching the energy dissipation over one oscillation from linear damping with damping coefficient B_{eq} and the energy dissipation from linear damping with damping coefficient B_{33} plus the quadratic drag force. Alternatively, it can be obtained by approximating the quadratic velocity term for drag force using the first term of its Fourier series (see, for example, Ref. [10]).

Both Eq. (1) and Eq. (2) are commonly used when modeling the loads on oscillating heave plates. When modeling heave plates in the HydroDyn hydrodynamics module of OpenFAST, either linear damping or quadratic drag force can be implemented. A combination of both is also possible. However, quadratic drag force is generally preferred because it also accounts for the background wave or current velocity by using the relative velocity between the structure and the background flow.

With deeply submerged heave plates, linear wave-radiation damping can be negligible. In this case, B_{33} can be neglected if the quadratic form drag dominates over the linear friction damping. This is usually true except for very small KC numbers. With B_{33} neglected, A_{33} and C_D can be found via Fourier decomposition of measured force time series from forced oscillation [14]. With a sinusoidal oscillation in calm water of amplitude a and angular frequency ω of the form

$$z(t) = a\sin(\omega t), \quad (4)$$

we have

$$A_{33} = \frac{1}{\pi a\omega}\int_0^T F_z(t)\sin(\omega t)\,\mathrm{d}t, \quad (5)$$

$$C_D = -\frac{3\omega}{4\rho S(a\omega)^2}\int_0^T F_z(t)\cos(\omega t)\,\mathrm{d}t, \quad (6)$$

where T is the period of oscillation, t is time, and F_z is the hydrodynamic force on the structure obtained from the measured force, F_3, with the known inertial and hydrostatic components subtracted out:

$$F_z = -A_{33}\ddot{z} - \frac{1}{2}\rho C_D S\dot{z}|\dot{z}|. \quad (7)$$

B_{eq} follows from C_D and Eq. (3) with B_{33} set to zero. Equivalently, if F_z is assumed to be of the form

$$F_z = -A_{33}\ddot{z} - B_{eq}\dot{z} \quad (8)$$

following Eq. (2), B_{eq} can be deduced from the force time series directly as

$$B_{eq} = -\frac{1}{\pi a}\int_0^T F_z(t)\cos(\omega t)\,\mathrm{d}t. \quad (9)$$

Instead of the dimensional added mass A_{33} and equivalent damping coefficient B_{eq}, the nondimensional coefficients of added mass, C_A, and equivalent linear damping, C_B, are often used. For this review, they are defined as follows:

$$C_A = \frac{A_{33}}{M'}, \quad (10)$$

$$C_B = \frac{B_{eq}}{2M'\omega}. \quad (11)$$

The reference mass, M', is based on the potential-flow added mass of a circular flat plate submerged in an infinite fluid [15]:

$$M' = \frac{1}{3}\rho D_h^3. \quad (12)$$

where the hydraulic diameter D_h is the diameter of the plate or the diameter of a circle with equivalent area if the plate is non-circular. Using the hydraulic diameter allows the performance of plates of different shapes to be directly compared.

We review prior publications to investigate the general dependence of C_A, C_B, and C_D on the various parameters characterizing the design of the heave plate and the conditions in which the heave plate operates. Two particularly relevant parameters are the KC number and the frequency parameter, β. For a structure undergoing forced oscillation, KC and β are respectively defined as

$$\mathrm{KC} = \frac{2\pi a}{D_h}, \quad (13)$$

$$\beta = \frac{{D_h}^2 f}{\nu}. \quad (14)$$

With offshore platforms, the motion of the structure is typically small compared to its dimensions; therefore, KC is generally low ($0 < \mathrm{KC} \leq 2$).

For systems strongly affected by viscous effects, Re is another important parameter. For an oscillating body, Re is defined as

$$\mathrm{Re} = \frac{2\pi a f D_h}{\nu} = \mathrm{KC} \cdot \beta. \quad (15)$$

Thus, Re is held constant as long as the product of KC and β is held constant.

Data were collected from figures presented in the literature. In the cases of C_A and C_B, the normalization of the coefficients is not always consistent between publications. Thus, all data are processed to follow the convention of Eq. (10) and Eq. (11) to be presented in a unified manner.

3. RESULTS AND DISCUSSION

This section summarizes data sourced from the references listed in Table 1 on the topic of oscillating underwater plates. In most cases, the experiments conducted involved a plate attached to a load cell and subjected to forced oscillation in calm water. Yang et al. [13] also numerically investigated forced oscillation in currents of varying speeds. The relevant hydrodynamic coefficients are analyzed with respect to their dependence on plate shape, KC, β, and the plate thickness ratio, $t' = t_p/D_h$.

Data collected from the literature show strong correlation between the added mass coefficient, C_A, and KC for circular and rectangular plates, as shown in Figures 2 and 3, respectively. To demonstrate the overall trend, C_A measured under different conditions and for different plate porosities are shown together.

In Figure 2, the results of Wadhwa and Thiagarajan [11] are those from experiments conducted at the deepest draft presented (20 cm; equal to the diameter of the plate) to minimize free-surface effects in the data shown. The data presented from Wadhwa et al. [12] are inclusive of all drafts considered because the effect of the tank bottom was small compared to the free-surface effects [11, 12]. The data from Tao and Dray [6] cover a range of plate porosity ratios from 0% to 20% and β varying from 1.6×10^4 to 1.6×10^5. For legibility, the results from the experiments conducted by Tao and Dray [6] are presented as the mean values of all experiments performed at a given value of KC along with the range of the data due to the inclusion of different plate porosities and values of β.

Despite the differences in the experimental setup, Bezunartea-Barrio et al. [2], Tao and Dray [6], Tian et al. [8], and Wadhwa et al. [12] all show linear relationships with similar values of $\frac{\partial C_A}{\partial \mathrm{KC}}$ over the range of KC number shown. On the other hand, Wadhwa and Thiagarajan [11] show a slightly greater $\frac{\partial C_A}{\partial \mathrm{KC}}$ that is likely caused by the difference in submergence. The data from Ref. [11] for different submergences (not shown) demonstrate a clear increase in $\frac{\partial C_A}{\partial \mathrm{KC}}$ with decreasing submergence. However, it should be noted that the experiments of Bezunartea-Barrio et al. [2] were performed at a smaller depth-to-diameter ratio of 0.775 compared to the unity ratio of Wadhwa and Thiagarajan [11] in Figure 2, yet the slope of Ref. [2] is closer to the rest of the data shown. The results from Ref. [2] might have been influenced by the presence of a large column (0.35 disk diameter) that the heave plate was attached to, which was not present in the other experiments in Figure 2.

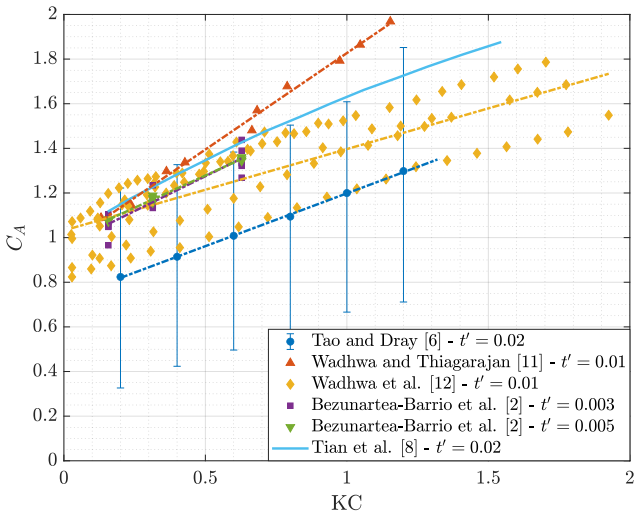

FIGURE 2: C_A AS A FUNCTION OF KC FOR CIRCULAR PLATES. "ERROR BARS" FOR TAO AND DRAY [6] ARE USED TO REPRESENT THE RANGE OF DATA FOR A SINGLE VALUE OF KC DUE TO DIFFERENT PLATE POROSITIES AND FREQUENCY PARAMETERS. TRENDLINES ARE PRESENTED TO ILLUSTRATE LINEAR RELATIONSHIP. THE RESULT FROM TIAN ET AL. [8] IS IN THE FORM OF A CURVE FIT.

As shown in Figure 3, Liang et al. [4] performed experiments with two square plates of equal area, with different plate thickness ratios of 0.022 and 0.066. Other than the thickness of the plates, the geometries of the plates and the tank conditions in which they were tested were identical. Figure 3 shows the two plates exhibiting similar added mass coefficients

at low values of KC with the thicker plate exhibiting less dependence on KC. Liang et al. [4] show evidence that suggests a possible relationship between the thickness ratio, t', and $\frac{\partial C_A}{\partial \mathrm{KC}}$. All other data sets included in Figure 3 are for plates with thickness ratios comparable to or lower than that of the thinner plate of Liang et al. [4], resulting in nearly identical values of $\frac{\partial C_A}{\partial \mathrm{KC}}$. Interestingly, despite the much lower added mass coefficient due to a 7.945% perforation ratio, the results of An and Faltinsen [1] show similar values of $\frac{\partial C_A}{\partial \mathrm{KC}}$ as the other thinner solid plates in Figure 3.

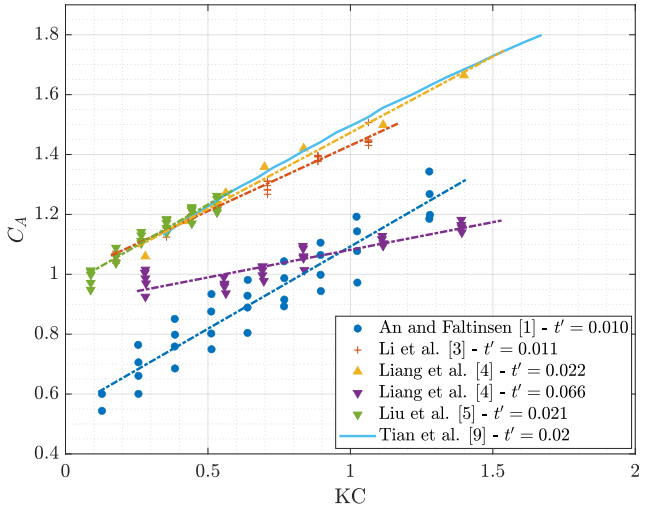

FIGURE 3: C_A AS A FUNCTION OF KC FOR RECTANGULAR PLATES. TRENDLINES ARE PRESENTED TO ILLUSTRATE LINEAR RELATIONSHIP. THE RESULT FOR A SQUARE PLATE FROM TIAN ET AL. [9] IS IN THE FORM OF A CURVE FIT. NOTE THAT KC IS RECOMPUTED FROM ITS ORIGINAL VALUES TO FOLLOW EQ. (13).

Figures 4, 5, and 6 show C_A as a function of β for circular plates. Similar to Figures 2 and 3, we are showing all data obtained under different conditions and for different plate designs together in order to demonstrate an overall trend. The KC number is controlled because of the strong dependence of C_A on KC, as demonstrated in Figure 2. Figures 4, 5, and 6, respectively, show data for low (KC ≤ 0.5), medium (0.5 < KC ≤ 1.0), and high (KC > 1.0) ranges of KC. Even when exercising control over KC, the dependence of C_A on β is less obvious compared to that on the KC number. There appears to be an overall trend of slightly decreasing C_A with increasing β for circular plates, which is most obvious with the data of Tao and Dray [6]. It should be noted that the dependence of C_A on β would strongly depend on the plate submergence, which is not controlled in Figures 4 through 6.

Figures 7, 8, and 9 show C_A as a function of β for rectangular plates. As with Figures 4, 5, and 6, the data are separated into groups of low (KC ≤ 0.5), medium (0.5 < KC ≤ 1.0), and high (KC ≥ 1.0) values of KC. As was the case with the data presented for circular plates, there does not appear to be a strong correlation between β and C_A for square plates at any level of KC based on the data shown.

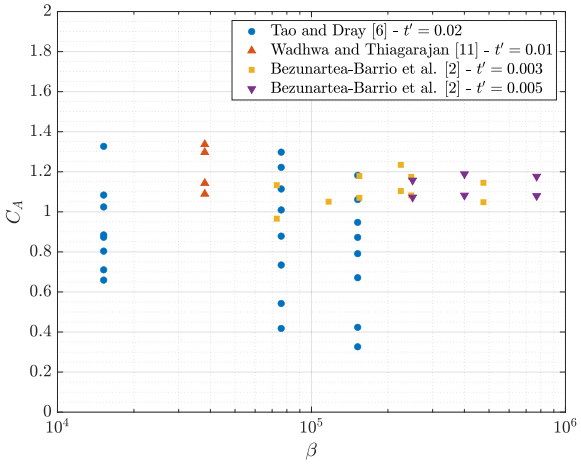

FIGURE 4: C_A AS A FUNCTION OF β FOR CIRCULAR PLATES, KC ≤ 0.5

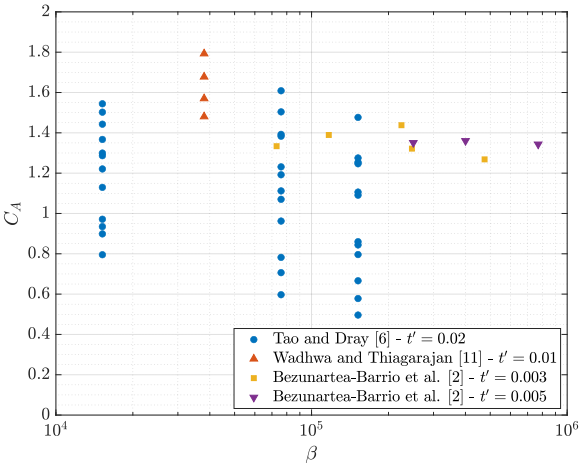

FIGURE 5: C_A AS A FUNCTION OF β FOR CIRCULAR PLATES, 0.5 < KC ≤ 1.0

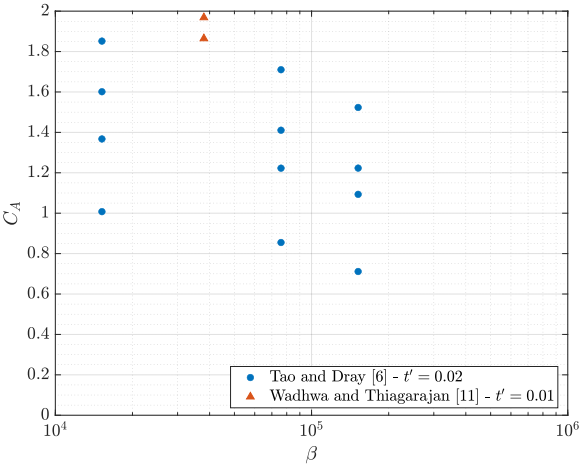

FIGURE 6: C_A AS A FUNCTION OF β FOR CIRCULAR PLATES, KC > 1.0

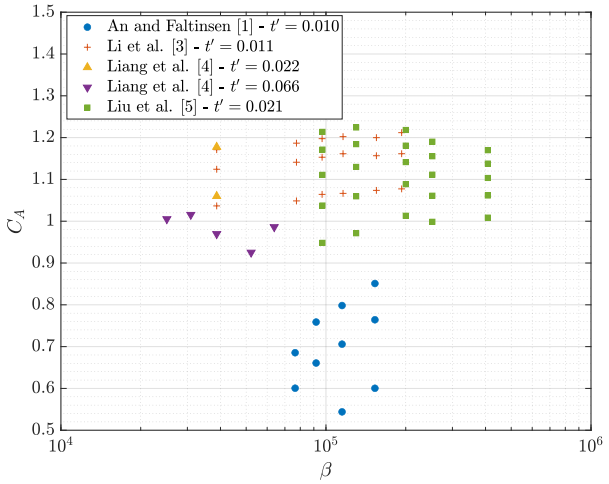

FIGURE 7: C_A AS A FUNCTION OF β FOR RECTANGULAR PLATES, KC ≤ 0.5

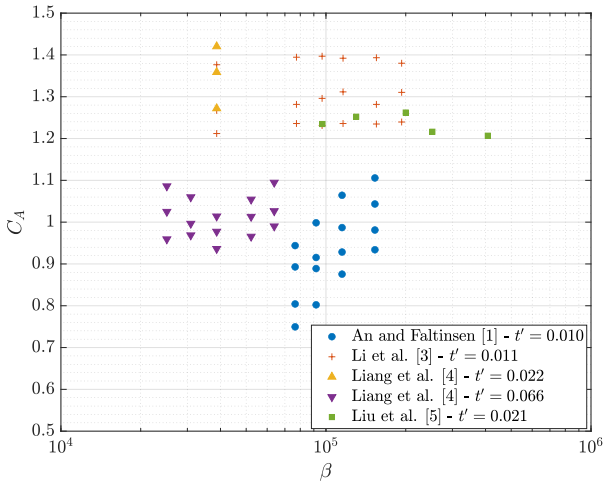

FIGURE 8: C_A AS A FUNCTION OF β FOR RECTANGULAR PLATES, 0.5 < KC ≤ 1

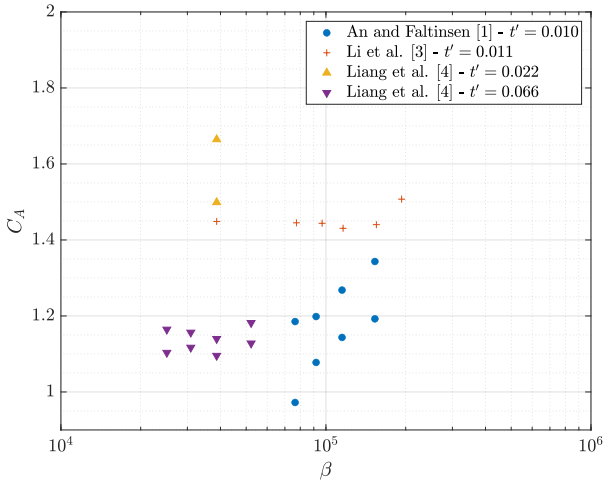

FIGURE 9: C_A AS A FUNCTION OF β FOR RECTANGULAR PLATES, KC > 1

Figure 10 shows data collected on the damping coefficient, C_B. As before, the results from Tao and Dray [6] cover plate porosities ranging from 0% to 20%. All other results are for solid plates. The results from Wadhwa et al. [12] for all different submergences are included. Intriguingly, there is consistent correlation between C_B and KC across experiments with different plate shapes and plate porosity.

As discussed in Tao and Thiagarajan [7], the primary mechanism driving the damping behavior of oscillating flat plates is the generation and shedding of vortices at the edge of the plate, which are most strongly influenced by KC and t'. It follows then that plates would experience similar damping characteristics so long as the edge conditions of the plates are similar. This also warrants further investigation of plates attached to the bottom of vertical cylinders or in very close proximity to the free surface or the basin bottom because the presence of the solid boundary or free surface can distort the formation and evolution of the shed vortices and impact the damping behavior.

The numerical investigation of Yang et al. [13] provides the only data set that includes the effects of current. The presence of current also affects the shedding and convection of vortices, which in turn, influences damping. High normalized current speed, V_R, tends to increase the damping of thicker plates ($t' \geq 0.1$). On the other hand, the damping of thinner plates ($t' = 0.02$) is more sensitive to the current; higher V_R can increase the damping at low KC but decrease the damping at high KC [13].

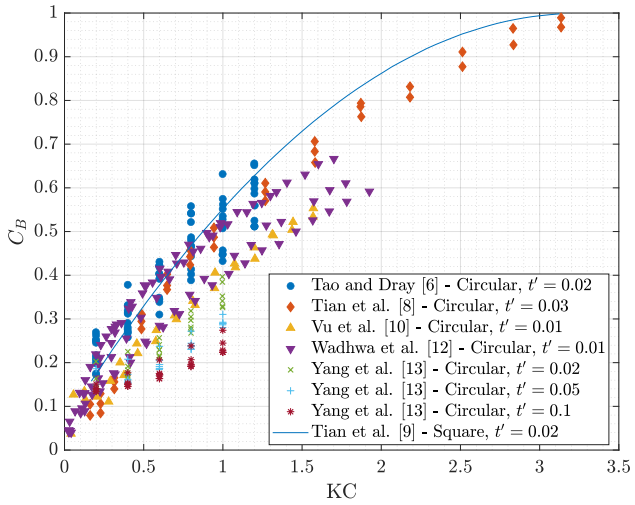

FIGURE 10: C_B AS A FUNCTION OF KC FOR CIRCULAR AND SQUARE PLATES. PLATE SHAPE IS NOTED IN THE LEGEND. THE RESULT FOR A SQUARE PLATE FROM TIAN ET AL. [9] IS IN THE FORM OF A CURVE FIT.

Figure 11 shows C_D for circular plates. Note that Refs. [8], [10], [12], and [13] do not provide C_D directly; the results shown are instead computed from the damping coefficient using Eq. (3). C_D decreases with increasing KC and converges toward just under 5 as KC exceeds 1. Increased scatter in the data is observed at lower KC values. There is also a correlation between the thickness ratio of a plate and C_D in Figure 11 as discussed in Ref.

[7]. Yang et al. [13] experimented with three different plate thicknesses, and the data show increasing C_D with decreasing plate thickness. This trend is more clearly observed with higher KC numbers.

Figure 12 shows C_D for solid square plates, which exhibits trends similar to those seen with circular plates; however, available data on C_D of square plates are more limited compared to circular plates. The data for square plates also suggest a correlation between plate thickness and C_D. The thickest square plate tested within the selected literature has a thickness ratio of 0.066 and was tested by Liang et al. [4]. It shows significantly lower values of C_D than the other square plates tested. The thinner plate tested by Liang et al. [4] and the plate tested by Liu et al. [5] are of comparable thickness ratios (0.022 and 0.021, respectively) and show similar C_D values, although the data from Liang et al. [4] show more variability coming from the effects of the frequency parameter, β. Both plates show higher C_D values overall than the thicker plate tested by Liang et al. [4]. The plate tested by Li et al. [3] is the thinnest of the square plates tested ($t' = 0.011$) and does not follow the pattern of C_D decreasing as plate thickness ratio increases. This plate shows C_D values higher than those of the thickest plate but lower than those of the other two. This suggests that other parameters might have a stronger impact on C_D for very thin plates.

Overall, the consistent trends of the hydrodynamic coefficients as functions of KC across a wide range of conditions and plate types are promising for the development of automated recommendation of hydrodynamic coefficients for heave plates in OpenFAST, at least when a suitable characteristic KC number exists and is known. However, it remains an open question whether and how a suitable KC number can be obtained under realistic conditions with motion excited by irregular waves because of the presence of motion and waves over a range of frequencies and because the motion of the structure is not known a priori. While the latter issue can be addressed through some iterative procedure in principle [16], the former requires further investigation (see Ref. [17] for some relevant discussions).

4. CONCLUSIONS

The data collected from the selected literature offer insight into the dependence of the hydrodynamic coefficients of heave plates on the relevant nondimensional parameters. The KC number has the strongest effect on the hydrodynamic coefficients. The added mass coefficient generally increases linearly with KC. There is also a correlation between the thickness of the plate and the rate at which C_A increases with the KC number. C_B also increases with increasing KC number, and the presence of current can influence the damping coefficient. The effect of proximity to the free surface or basin bottom and that of the presence of a column on C_B warrant further investigation. Finally, C_D decreases with the KC number. Increased scatter in C_D is observed with lower KC numbers, and C_D tends to converge toward just under 5 for higher KC numbers (KC > 1) across a range of conditions and plate types. A decrease in C_D with increasing plate thickness is also observed when all other factors are the same.

Overall, the mostly consistent trends of the various hydrodynamic coefficients across different heave-plate geometries and types suggest it might be possible to develop a capability within OpenFAST to automatically recommend and adjust hydrodynamic coefficients for heave plates based on the KC number. However, it remains an open question whether and how a suitable KC number can be determined under realistic conditions with motion excited by irregular incident waves.

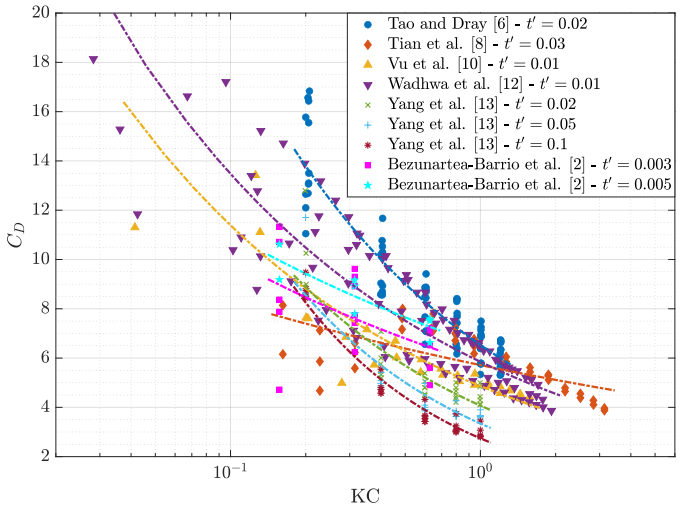

FIGURE 11: C_D AS A FUNCTION OF KC FOR CIRCULAR PLATES. TREND LINES ARE ADDED FOR VISUAL CLARITY ONLY.

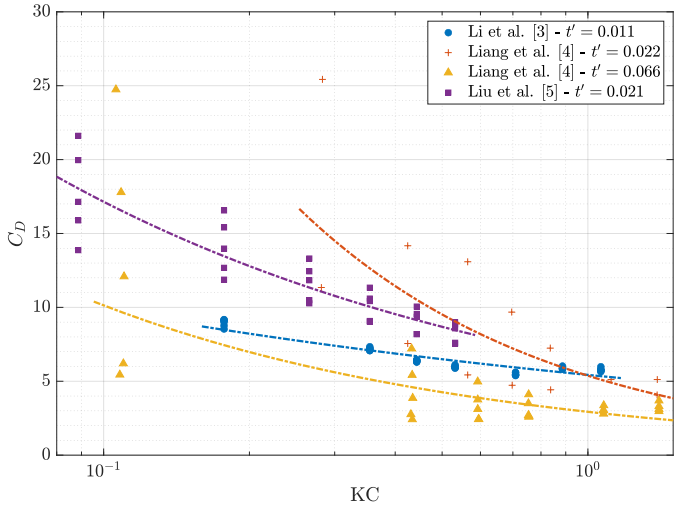

FIGURE 12: C_D AS A FUNCTION OF KC FOR SQUARE PLATES. TREND LINES ARE ADDED FOR VISUAL CLARITY ONLY. NOTE THAT KC IS RECOMPUTED FROM ITS ORIGINAL VALUES TO FOLLOW EQ. (13).

In the future, more data from the literature will continue to be collated to form a comprehensive database on heave-plate hydrodynamic coefficients. Detailed least squares regression analyses will also be performed on this database to illustrate the

effects of each individual parameter on the hydrodynamic coefficients. The applicability of empirical formulae for the hydrodynamic coefficients from the literature will also be evaluated using this database. Finally, it is of interest to investigate the influence of other platform components on the hydrodynamic coefficients of heave plates, including columns and pontoons, because, in practice, heave plates never operate in isolation and are always part of a complex structure.

ACKNOWLEDGEMENTS

This work was authored in part by the National Renewable Energy Laboratory, operated by Alliance for Sustainable Energy, LLC, for the U.S. Department of Energy (DOE) under Contract No. DE-AC36-08GO28308. Funding provided by the U.S. Department of Energy Office of Energy Efficiency and Renewable Energy Wind Energy Technologies Office. The views expressed in the article do not necessarily represent the views of the DOE or the U.S. Government. The U.S. Government retains and the publisher, by accepting the article for publication, acknowledges that the U.S. Government retains a nonexclusive, paid-up, irrevocable, worldwide license to publish or reproduce the published form of this work, or allow others to do so, for U.S. Government purposes.

REFERENCES

[1] An, S. and Faltinsen, O.M., (2013), "An experimental and numerical study of heave added mass and damping of horizontally submerged and perforated rectangular plates." *J. Fluids Struct.*, Vol. 39, pp. 87-101.

[2] Bezunartea-Barrio, A., Fernandez-Ruano, S., Maron-Loureiro, A., Molinelli-Fernandez, E., Moreno-Buron, F., Oria-Escudero, J., Rios-Tubio, J., Soriano-Gomez, C., Valea-Peces, A., Lopez-Pavon, C., and Souto-Iglesias, A., (2020), "Scale effects on heave plates for semi-submersible floating offshore wind turbines: case study with a solid plain plate," *J. Offshore Mech. Arct. Eng.*, Vol. 142, p. 031105.

[3] Li, J., Liu, S., Zhao, M., and Teng, B., (2013), "Experimental investigation of the hydrodynamic characteristics of heave plates using forced oscillation," *Ocean Eng.* Vol. 66, pp. 82-91.

[4] Liang, H.-Z., Liu, K., Li, L.-Y., and Ou, J.-P., (2018), "Dynamic performance analysis of the tuned heave plate system for semi-submersible platform," *China Ocean Eng.* Vol. 32, pp. 422-30.

[5] Liu, K., Liang. H., Ou, J., Ye, J., and Wang, D., (2022), "Experimental investigation of the performance of a tuned heave plate energy harvesting system for a semi-submersible platform," *J. Mar. Sci. Eng.* Vol. 10, p. 45.

[6] Tao, L. and Dray, D, (2008), "Hydrodynamic performance of solid and porous heave plates," *Ocean Eng.*, Vol. 35, pp. 1006-14.

[7] Tao, L. and Thiagarajan, K., (2003), "Low *KC* flow regimes of oscillating sharp edges. II. Hydrodynamic forces," *Appl. Ocean Res.*, Vol. 25, pp. 53-62.

[8] Tian, X., Yang, J., Li, X., and Peng, T., (2013), "Experimental investigations on the hydrodynamic characteristics of heave plate," in *Proceedings of the ASME 2013 32nd International Conference on Ocean, Offshore and Arctic Engineering*, Nantes, France, p. V005T06A032.

[9] Tian, X., Tao, L., Li, X., and Yang, J., (2016), "Hydrodynamic coefficients of oscillating flat plates at $0.15 \leq KC \leq 3.15$," *J. Mar. Sci. Tech.*, Vol. 22, pp. 101-13.

[10] Vu, K.H., Chenu, B., and Thiagarajan, K.P., (2008), "Hydrodynamic damping due to porous plates," in *Proceedings of World Scientific and Engineering Academy and Society*, Corfu, Greece.

[11] Wadhwa, H. and Thiagarajan, K.P., (2009), "Experimental assessment of hydrodynamic coefficients of disks oscillating near a free surface," in *Proceedings of the ASME 2009 28th International Conference on Ocean, Offshore and Arctic Engineering*, Honolulu, Hawaii, USA, pp. 435-41.

[12] Wadhwa, H., Krishnamoorthy, B., and Thiagarajan, K.P., (2010), "Variation of heave added mass and damping near seabed," in *Proceedings of the ASME 2010 29th International Conference on Ocean, Offshore and Arctic Engineering*, Shanghai, China, pp. 271-77.

[13] Yang, J., Tian, X., and Li, X., (2014), "Hydrodynamic characteristics of an oscillating circular disk under steady in-plane current conditions," *Ocean Eng.*, Vol. 75, pp. 53-63.

[14] Keulegan, G.H. and Carpenter, L.H., (1958), "Forces on cylinders and plates in an oscillating fluid." *J. Res. National Bureau of Standards*, Vol. 60, pp. 423-40.

[15] Sarpkaya, T., (2010), *Wave forces on offshore structures.* Cambridge University Press.

[16] Lemmer, F., Yu, W., and Cheng, P.W., (2018), "Iterative frequency-domain response of floating offshore wind turbines with parametric drag." *J. Mar. Sci. Eng.*, Vol. 6, p. 118.

[17] Wang, L., Robertson, A., Jonkman, J., and Yu, Y.-H., (2022), "OC6 Phase I: Improvements to the OpenFAST predictions of nonlinear, low-frequency responses of a floating offshore wind turbine platform." *Renew. Energy*, Vol. 187, pp. 282-301.